Correlative imaging of motoneuronal cell elasticity by pump and probe spectroscopy

Ahmed Hamraoui, Océane Sénépart, Maxime Schneider, Sophie Malaquin, Emmanuel Péronne, Loïc Becerra, Fannie Semprez, Claire Legay, Laurent Belliard

▶ **To cite this version:**

Ahmed Hamraoui, Océane Sénépart, Maxime Schneider, Sophie Malaquin, Emmanuel Péronne, et al.. Correlative imaging of motoneuronal cell elasticity by pump and probe spectroscopy. Biophysical Journal, 2021, 10.1016/j.bpj.2020.12.021 . hal-03105912

HAL Id: hal-03105912
https://hal.science/hal-03105912

Submitted on 18 May 2021

HAL is a multi-disciplinary open access archive for the deposit and dissemination of scientific research documents, whether they are published or not. The documents may come from teaching and research institutions in France or abroad, or from public or private research centers.

L'archive ouverte pluridisciplinaire **HAL**, est destinée au dépôt et à la diffusion de documents scientifiques de niveau recherche, publiés ou non, émanant des établissements d'enseignement et de recherche français ou étrangers, des laboratoires publics ou privés.

Correlative imaging of motoneuronal cell elasticity by pump and probe spectroscopy

Ahmed Hamraoui*[1,5], Océane Sénépart[1,3,4], Maxime Schneider[1,3,4], Sophie Malaquin[2], Emmanuel Péronne[2], Loïc Becerra[2], Fannie Semprez[3], Claire Legay[3], and Laurent Belliard[2]

[1]Sorbonne Université, CNRS, Collège de France, UMR7574, Laboratoire de Chimie de la Matière Condensée de Paris, 4 place Jussieu, 75005 Paris, France
[2]Sorbonne Université, CNRS UMR7588, Institut des Nanosciences de Paris, 4 place Jussieu, 75005 Paris, France
[3]Saints-Pères Paris Institute for the Neurosciences, CNRS UMR 8003, Université de Paris, Paris Descartes, Faculté des Sciences Fondamentales et Biomédicales, 45 rue des Saints-Pères, 75006 Paris, France
[4]Centre de recherche de l'ECE Paris-Lyon, Immeuble Pollux - 37 quai de Grenelle - CS 71520 - 75015 Paris, France
[5]Université de Paris, Paris Descartes, Faculté des Sciences Fondamentales et Biomédicales, 45 rue des Saints-Pères, 75006 Paris, France

Abstract

Because of their role of information transmitter between the spinal cord and the muscle fibers, motor neurons are subject to physical stimulation and mechanical properties modifications. We report on motoneuron elasticity investigated by time resolved pump and probe spectroscopy. A dual picosecond geometry probing simultaneously the acoustic impedance mismatch at the cell/Titanium transducer interface and acoustic wave propagation inside the motoneuron is presented. Such non-contact/non-destructive microscopy, correlated to standard atomic force microscopy or fluorescent labels approach have been carried out on a single cell to address some physical properties as bulk modulus of elasticity, dynamical longitudinal viscosity or adhesion.

Statement of Significance

Many cellular processes trigger changes in the elastic properties of cells and their viscosity. It is often difficult to say whether changes in the stiffness of cells or tissues result from or are the cause of diseases. This is why the detailed description of the mechanical properties of the cells is necessary to know their behavior during the development or the death of the cells. This research requires non-invasive techniques to probe and quantify locally their mechanical properties at the single-cell scale. In this article we report on motoneuron elasticity investigated by time resolved pump and probe spectroscopy. We address in an integrated way the questions raised about the mechanical characteristics of a motoneuronal cells. At the peripheral of the motoneuron, we evaluated sound velocity for this rich actin zone which allowed us to the identification of the structure of the cell, highlighting a nucleus characterized by high rigidity and a lower viscosity than the rest of the cell. We also found that the growth cone exhibits higher sound velocity than the motoneuronal cell body. The attenuation of the Brillouin signature gives access to dynamical longitudinal viscosity of the motoneuron. Different areas were distinguished inside the cell. The nucleus material shows a bulk modulus higher than the rest of the cell.

1 INTRODUCTION

The motor system is a complex structure connecting the central and peripheral systems. The activity of this system is responsible for skeletal muscle movement, a function that is indispensable for life. Its

*correspofnding author

activity relies on convergent neuronal networks integrating the functions of a number of structures from brain to skeletal muscles. The central processing unit that receives instructions from the brain is the motor neurons whose cell bodies are located in the spinal cord and the targets they innervate are found in the muscles. Neuronal information is transmitted to the muscle at the neuromuscular junction, a chemical synapse that uses acetylcholine as a neurotransmitter in vertebrates. Motor neurons, like any other cells are active materials that can detect mechanical stimulation, generate and tolerate mechanical forces within their environment and also respond to physical cues through cytoskeletal (re)organization as part of their physiological activities. This is made possible by the activation of mechanically sensitive signaling pathways. Any changes in the architecture of the cytoskeleton can lead to changes in the mechanical properties of cells, such as elasticity, adhesiveness and viscosity, and defects in adaptations to mechanical stimuli can result from genetic mutations and pathogens in cytoskeletal components. The motor system and in particular the motor unit composed of the motoneuron and the innervated muscle is the target of high tension generated by repeated muscle contractions. This is why the mechanical properties of motor neurons are of great interest for understanding the development, the establishment of neuromuscular junctions and the behavior of motor neurons. Mechanics and cell adhesion are today a promising subject in cell research because cell mechanics can bear witness to its vitality and state of health and cell adhesion is at the heart of many processes and cycles that rule his life.

The vast majority of conventional methods for measuring the local mechanical properties of cells [1, 2] or applying forces on them [3] are based on the use of solid probes, such as atomic force microscopy (AFM). Nevertheless, quantitative estimation of the cell mechanical properties by such methods is made difficult by adhesion interactions between the local probe and the cell but also by the role played by the substrate. In this context, contactless methods are of major interest. Acoustic microscopy which captures images of the mechanical properties of a material without being destructive, seems to be an adequate tool for such studies. Acoustic microscopy can be used to determine acoustic velocities, densities, thicknesses or even acoustic attenuation inside the neuronal material [4, 5]. From the first applications of acoustic microscopy, the measurements carried out have shown the non-invasive potential of assessing mechanical properties on a local scale in the cell as well as applications to cell imaging [6, 7]. However, the application of acoustic microscopy on single cells is still tricky because the resolution limits at room temperature of this technique are the size of the cells, or even above.

It therefore seems that picosecond acoustics can offer many advantages for the study of cellular mechanics. It is indeed the only acoustic measurement technique which allows optical generation and detection of acoustic waves of frequency up to THz, and which can therefore make it possible to obtain acoustic images whose resolution is significantly lower than the cell thickness [8].

Although Brillouin Light Scattering represent a powerful approach to address biological issues specially in living cell [9], an alternative approach based on high frequency coherent acoustic waves generated by femtosecond lasers provide a very adequate tool for probing the mechanical properties of biological cells or tissues in a non-contact and non-invasive configuration. The main advantage is then to amplify the Brillouin scattering using coherent phonons rather than applying the thermal phonons. Moreover, time resolved pump and probe spectroscopy allow to get the sound velocity with a high accuracy ($< 5\%$) which is one of the crucial parameters for elasticity issues. The oscillating response of the sample reflectivity resulting from the interaction between light and the acoustic pulse propagating into the cell, usually called the Brillouin oscillations (BO) has demonstrated ability to map elasticity in biological cells. In-plane or in-depth investigations [10, 11, 12, 13, 14] can reveal the internal elasticity gradient and thickness of the cell. Such all optical technique is very convenient to design specific environment allowing the study of living cells [15, 16]. Additionally, acoustic pulse probed after its reflection at the interface between the cell and the substrate gives access to acoustic mismatch and to physical characteristics of the contact between the cell and the substrate [17, 18, 19]. Recently, a multi parametric elastic mapping combining these different approaches have been reported in mitotic macrophages cell [20].

In the present paper, we develop a correlative approach coupling acoustic impedance, Brillouin signature, and attenuation mapping to AFM investigations and fluorescence labelling over the same motoneuronal cell. Both bulk modulus and viscoelastic properties in the nucleus and the cytoskeleton are thus clearly visualized and quantified.

2 MATERIAL AND METHOD

2.1 Cells and substrate

The motoneurons used in this study are immortalized mouse motoneurons called $MN1$. They are cultured on biocompatible titanium layer sputtered on sapphire substrate 3 days before fixation. Fixation was performed with glutaraldehyde [2% in phosphate-buffered saline (PBS)] at room temperature during $15 - 20min$. Cells were washed twice with PBS for $5\,min$, quickly rinsed with deionized water to remove salts and then dried under a moderate stream of nitrogen.

For immunohistochemistry, cells were incubated overnight at $4°C$ with a rabbit polyclonal anti-beta actin ($1\,\mu g.mL^{-1}$; *abcam ab*8227). Three $10\,min$ washes were carried out with PBS tween 0.1% . Cells were then incubated $1\,h$ at room temperature with a secondary antibody coupled to alexa fluor 488 goat anti rabbit at dilution 1/500 (thermo fisher scientific: 10729174). Nuclei were labelled with DAPI.

The layer thickness is fixed at $300\,nm$ in order to observe consecutive and well separated echoes. Some additional numbers have been printed in gold by standard lift-off process, those structures allowed to localize the cell at the surface. It is then possible to perform different kind of experiments like acoustic, fluorescence and atomic force microscopy over the very same cell.

The motoneurons studied were fixed, after which the cells cannot be active anymore but retained most of their morphological characteristics. This protocol makes it possible to carry out studies in the open air without degradation of the cell and without them moving during the acoustic acquisition. The effect of cell fixation on the mechanical properties of the cell is not perfectly known, but the cell is supposed to keep the same differential in mechanical properties in fixed condition and *in-vitro*.

2.2 Experimental set-up

Ultrafast pump-probe spectroscopy experiments are performed in standard synchronous scheme using a mode-locked Ti: sapphire (MAI-TAI Spectra) laser source operating at $800\,nm$ with a pulse duration of $100\,fs$ at a repetition rate of $78.8\,MHz$. The pump beam is modulated at $1.8\,MHz$ to perform synchronous detection on the sample reflectivity. Both pump and probe beams are focused by an objective with a $NA = 0.5$ and are normally incident on the sample. More details about the pump and probe set-up could be found in references [21, 22].

To avoid scattered light coming from the pump beam, a two-color experiment is performed by doubling the probe frequency ($\lambda = 400nm$) with a nonlinear crystal. A dichroic filter located in front of the diode system suppresses the light of the pump beam, its power is reduced around $300\,\mu W$ and the power of the probe beam does not exceed $30\,\mu W$. With such experimental conditions, we stay in the thermo-elastic regime, the acoustic signal and the optical reflectivity remain stable during all the average processing. Moreover, due to the high thermal conductivity of the sapphire substrate the cell heating could be neglected. The main specificity of this set up is the ability to perform simultaneously experiment in reflection and in transmission geometry see figure 1, in order to reach a multi-parameter investigation. In both sizes, the sample reflectivity is measured by an avalanche photodiode and analyzed using a lock-in amplifier.

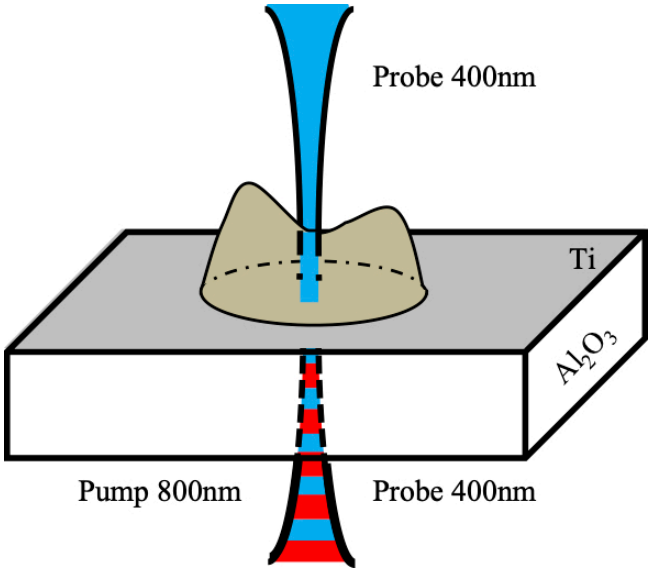

Figure 1: Reflection and transmission configuration. In reflection, the acoustic echo after their reflection at the interface Ti/air or $Ti/cell$ are detected. In transmission the propagation of the acoustic pulse transmitted into the cell is measured.

After performing the pump and probe alignment in both sizes, the sample is scanned using an $X-Y$ piezoelectric stage in order to perform acoustic mapping of the motoneurons selected .

2.3 Atomic Force Microscopy

MN1 cells cultured on Ti layer were imaged using a Digital Instruments AFM (Veeco). Ambient AC mode was used with Veeco RTESP tip cantilevers spring constant : $4\,N\cdot m^{-1}$ and 256 lines 512 pixels images were acquired at a scanning frequency of $1-2\,Hz$. The system includes an integrated optical microscope, allowing prepositioning of the AFM tip over the cells. Using a profile section coupled to an average process in the cell, we can estimate cell thickness at specific peripheral locations in order to correlate them with time of flight.

3 RESULTS

First, we will consider the results obtained in reflection geometry where the acoustic pulse is generated at the $Ti/sapphire$ interface. After its propagation in the Ti layer and being reflected at the Ti/air or $Ti/cell$ interface (figure 1), this acoustic wave is detected by the probe at the Ti/sapphire interface. In figure 2, superimposed on the decaying thermal background we can observe a high frequency component associated to Brillouin detection in the transparent sapphire substrate. Additionally, first and second echo signatures are clearly visible with inverse sign as expected accordingly to the higher acoustic impedance of the sapphire substrate. The separation time is in good agreement with a longitudinal sound velocity equal to $6.2\,nm/ps$ in titanium transducer, extracted from pulse echo measurements made in a series of Ti layers with controlled variable thickness. As underlined in figure 2, the echoes exhibit lower amplitude when the measurements are performed below the cell. The acoustic reflection coefficient is then lower for $Ti/cell$ interface compare to its counterpart equal to 1 for Ti/air interface.

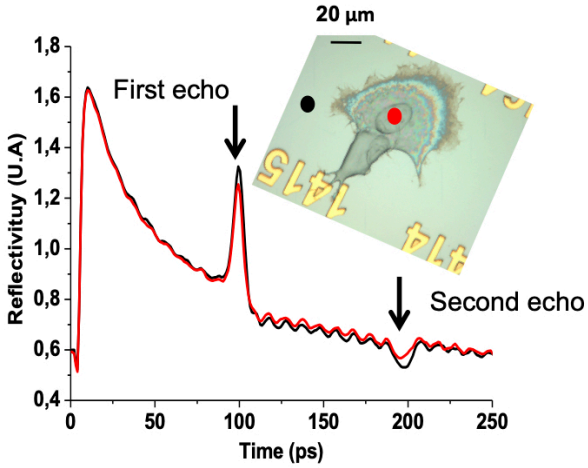

Figure 2: Comparison between sample reflectivity measured outside (Black) and underneath the motoneuron (Red). The two transient signals are similar expected the amplitude of the two echoes pointed out by arrows. Inset : Optical image of the cell. The black curve is measured far from the cells at the Ti/air interface while the red curve, with a slightly lower echo amplitude, represents the signature of the Ti/cell interface.

In recording reflectivity mapping at different pump probe delays around the first echo, similar transient signals could be obtained at all locations outside and inside the studied cell. This work has been done using 90 images delayed by $1\,ps$ between time delays equal to $60\,ps$ up to $150\,ps$. Each image is composed by $60 \times 60 pixels$ for a total scale of $91\,\mu m$. The pixel size chosen in the following acoustic maps is close to the resolution estimated from the pump and probe beam profile of $1.5\,\mu m$. Such experiment required $2\,h$. In figure 3a such mapping is presented for a time delay corresponding to the detection of the first echo. As expected, the whole cell in contact with the Ti layer is assigned by a lower signal. From this 3600 time resolved signatures deduced, we can compute the ratio R between the first echo amplitude over a reference signal measured outside the cell. Finally, a mapping of the acoustic cell impedance is obtained in figure 3b using the following equation, expected for a perfect cell adhesion [23]:

$$R = \frac{Z_{Ti} - Z_{cell}}{Z_{Ti} + Z_{cell}} \tag{1}$$

with Zi the acoustic impedance of the different layers given by the product of the density and the longitudinal velocity, $Z_{Ti} = 4.5 \times 6.2\,MPa \cdot s \cdot m^{-1}$.

The treatment performed to obtain the figure 3b is not relevant for the points located under the gold label, where the first echo exhibits an inverse polarity. The average cell acoustic impedance is founded equal to $3.05\,MPa{\cdot}s{\cdot}m^{-1}$, meaning a longitudinal sound velocity equal to $3.05 \pm 0.1\,nm{\cdot}ps^{-1}$ assuming a density of 1. The bulk modulus $B = \rho v^2$ associated is equal to $9.3\,GPa$. Possible fluctuations versus frequency component of the acoustic pulse has been reached in order to quantify adhesion aspect between cell and Ti layer [19, 20]. Nevertheless, no clear frequency dependence has been detected testifying a good uniform cell adhesion with titanium underlayer [24, 25, 26].

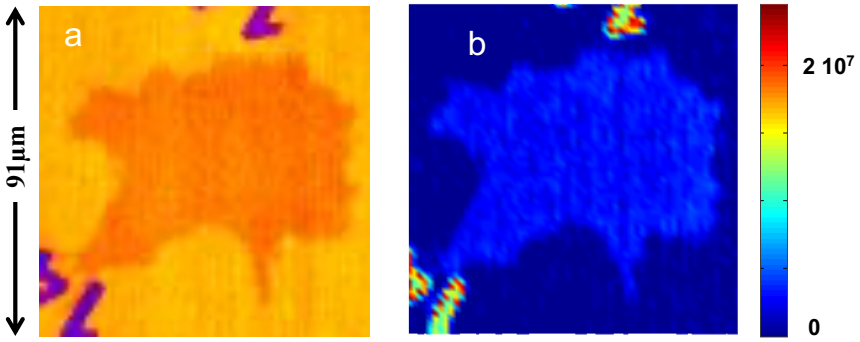

Figure 3: a) Mapping of the transient reflectivity sample measured at a delay 97.1ps (scale 91μm). In such image the cell is clearly pointed out by a smaller amplitude of the echo due to acoustic energy transmission into the cell body. b) Mapping of the acoustic impedance deduced from the echo amplitude at the interface between the Ti transducer and cell. Unit in $MPa \cdot s \cdot m^{-1}$.

The figure 4a is extracted from the previous image stack for a delay equal to 23 ps after the main first echo. On this acoustic mapping, we can notice a small additional white feature located at the upper cell periphery where the filopods of the "growth cone" which represents the tip of the axon extends and this zone is therefore thinner with a high actin density.

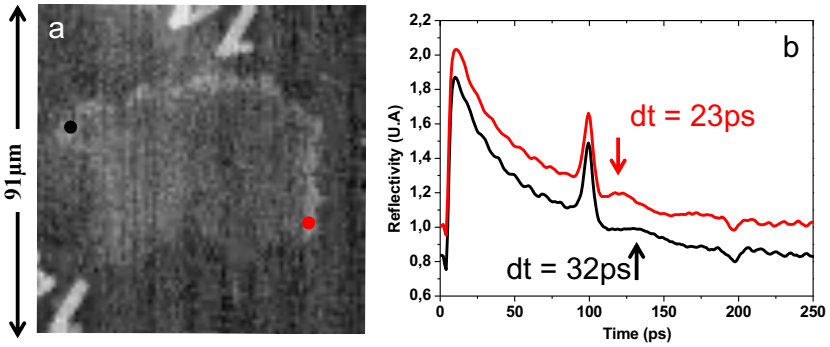

Figure 4: a) Mapping of the acoustic signature 23 ps after the first main echo coming from the $Ti/cell$ interface. A small signal is clearly visible in the upper periphery of the cell. b) Time resolved signature have been recorded in two locations on this specific area. The additional bump emerges a different time delay versus the location. The two curves have been slightly shifted for a better visibility.

In order to get insight into this new signature, time resolved measurements have been performed on this specific area, see figure 4b. As expected from the mapping, an additional bump emerges few picoseconds after the first echo. The time location of this broad signature is also strongly correlated to the location of measurements.

Such slightly delayed feature may be assigned to a round trip in the thin cell periphery of the transmitted acoustic pulse. To determine the sound velocity, the knowledge of the cell thickness is crucial, consequently atomic force mapping have been realized on the same cell. In order to get the profile section, AFM images in tapping mode have been recorded on the studied areas (see figure 5).

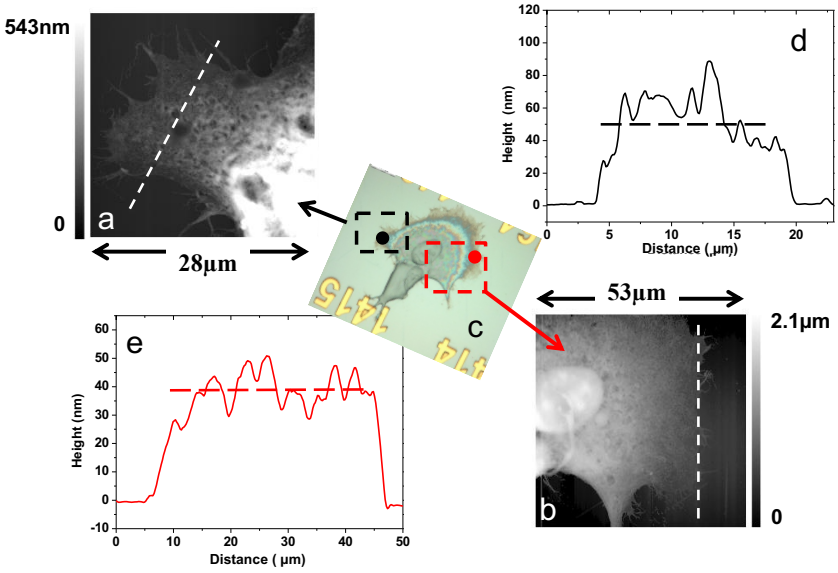

Figure 5: a-b) Atomic force image, in tapping mode, with 28 and 53 μm scale respectively. c) Optical image d-e) Profile section obtained where the pump and probe presented in figure 4 have been performed. The average height is 40 nm and 50 nm associated to bump delayed by 23 ps and 32 ps respectively.

The profiles reveal a large cell roughness which could be responsible for a broadening and attenuation of the measured acoustic features. However, the average thickness can be evaluated and then compared to the time delays as measured by the pump and probe technique. The sound velocity for this rich actin zone may be estimated around $3.3 \pm 0.2\, nm \cdot ps^{-1}$, given a bulk modulus equal to $10.9\, GPa$

The growth cone clearly exhibits higher sound velocity than the motoneuronal cell body in the cell center. Such discrepancy leading to a stiffness greater than 20% in the rich and ordered actin zone as previously expected from [27, 28].

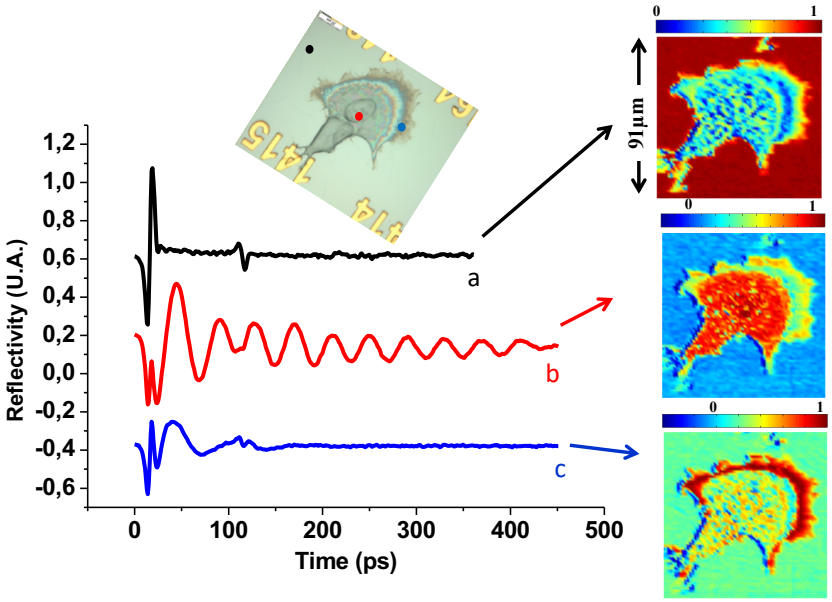

Figure 6: a) Series of time resolved signals measured at three different spots labeled a) b) and c), showing echoes and Brillouin standard features. The top inset displays the optical image of the cell and the three measured area located with dots: a) at the free surface. b) in the core cell. c) at the cell periphery. On the right the Pearson correlation mapping associated to the three spots respectively.

As previously described, a series of 150 images with a time separation of 4 ps have been performed

to probe the Brillouin signature of the cell under studied. In order to single out the typical features which are observed in motoneurons, the pump-probe signal of three different spots are emphasized in figure 6. In this transmission scheme, the echoes emerging at the free surface are detected as transient repetitive signals separated by $97.5\,ps$ as in reflectivity geometry, figure 6a. When the probe is focus on the cell, the acoustic pulse transmitted into the cell body gives an additional oscillation feature usually called Brillouin oscillation, figure 6b. This periodic signal results from interference between light reflected by the propagating acoustic wave front and the light reflected by the Ti surface. The frequency fb of this new component gives a direct access, across the sound velocity, to the cell elasticity using the following equation 2:

$$f_b = \frac{2\,n\,V}{\lambda} \tag{2}$$

where n is the optical cell index, λ the laser wavelength and V the longitudinal sound velocity.

In such a detection scheme, the BO decay time may be related to intrinsic attenuation associated to dynamical viscosity [12, 29]. To unambiguously determine the Brillouin frequency and decay time, the cell should be thicker than the acoustic wavelength into the cell which is equal to half of the laser wavelength inside the cell, i.e. $200\,nm$. Consequently, since the cell thickness at spot c in figure 6 is shorter than the acoustic wavelength(see figure 5), the oscillating signal corresponding to the cell periphery (see figure 6c), cannot be ascribed to a bare Brillouin oscillation. It is more likely explained by the photo-elastic detection of the breathing modes of the thin actin layer rather than the detection of a progressive wave (which is the case for pure Brillouin oscillation).

Following a previous work [12], the Pearson correlation image have been computed and drawn in the right panel of figure 6 for the three representative time resolved signals. We find a very good correlation between all pump-probe signal recorded outside the cell. Within the cell, two main zones are identified, the thin cell periphery and the cell body. In the cell body a blurred area suggests different inner structures. To clarify this view, the figure 7a gives the exponential time decay mapping of the BO within the cell.

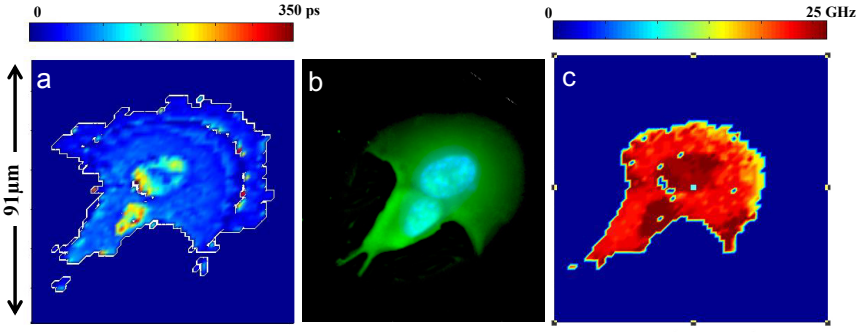

Figure 7: Image scale $91\,\mu m$. a) Mapping of the Brillouin life time in the cell. b) Fluorescence mapping of the same cell. The blue zone marked the nucleus material and the green color pointed out the cytoskeleton rich in Actin. c) Mapping of the Brillouin frequency cell response. The values are fixed at zero outside the motoneuron where no Brillouin oscillation are detected.

This image reveals two areas which exhibit decay time larger than 175 ps in contrast with their surrounding showing shorter decay time (*i.e.* higher attenuation). These globular zones are also highlighted in the Brillouin frequency mapping after the treatment of the image stacking, figure 7c. Indeed, we clearly underline the same areas associated to high Brillouin frequency $25\,GHz$, compared to the surroundings given around $22\,GHz$. In the frequency mapping, we have excluded the points where the time decay is lower than the Brillouin periodicity, then the whole cell surface does not appear. In other words, the signal recorded in the transmission scheme at the periphery of the cell is not considered sufficiently relevant to extract information on the elasticity of the cell with the help of Brillouin oscillation fitting. This drawback is partly circumvented by the results reported in reflection geometry in this rich actin zone. In order to associate these acoustic structures to specific zones of the cell, we resorted to a well- known technique, the fluorescence microscopy which allowed to distinguish the nucleus from the surroundings cytoskeleton, figure 7b. As expected the nucleus are located at

position where the Brillouin frequency is higher and the cytoskeleton where the Brillouin frequency is lower within the cell.

Assuming a constant optical index and density equal to 1.35 [30, 31, 32] and $10^3\,kg{\cdot}m^{-3}$, respectively a bulk modulus of $13.7\,GPa$ or $10.6\,GPa$ can be extracted. These values are close to those recently obtained in PC12 neuron-like cells models [12]. The bulk velocity extracted outside the core cell, equal to $3.25 \pm 0.5 nm \cdot ps^{-1}$ is slightly higher than the velocity estimated from the acoustic mismatch testifying that the membrane is characterized by a weaker stiffness than the rest of the cell. On this crucial point, we had to keep in mind that we are handling high frequency acoustic waves (GHz range) therefore it is well known that in viscoelastic materials (such as cells for example) there is a strong frequency dependence of the elastic modulus. It is therefore expected to obtain values much higher than those obtained by static methods. Nevertheless, the elastic contrast remains a signature of the internal structure of the neuron and of a possible modification linked to the environment or to a pathology.

Moreover, the fluctuation of the dynamical longitudinal viscosity μ can be evaluated as well, given that the lifetime of the Brillouin oscillation is expressed as $\tau = \dfrac{\rho V^2}{4\pi^2 f_b^2 \mu}$ [33]. The deduced viscosity in the core cell is estimated at $3.2\,mPa \cdot s$ twice as low as in the cytoskeleton where the attenuation is more pronounced. The uncertainty on this value is directly linked to the distribution of the attenuation in the areas studied, i.e. around 25%. Those values are been measured on different moto-neurons and are pretty consistent (within the precision addressed above). To illustrate this, the Brillouin frequency mapping obtained on another cell is compared with in homogeneous media its corresponding fluorescence mapping in figure 8. In this case, cell fixation occurred at the mitosis stage, as evidenced by its form of bilobed nucleus.

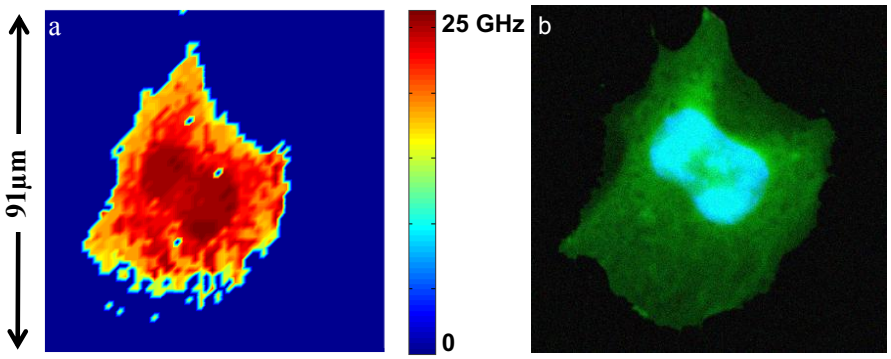

Figure 8: Image scale $92\,\mu m$. a) Mapping of the Brillouin frequency cell response. The nucleus, pointed out by a higher stiffness, has been fixed during its differentiation process as evidenced by its two-lobed form. b) Fluorescence mapping of the same cell.

CONCLUSION

Tissue stiffness, when disturbed, can be associated with different forms of pathology. But we cannot conclude whether this change in tissue stiffness is the consequence or the origin of the pathologies. Therefore, characterization of the mechanical properties of cells / tissues is essential to understand their behavior during cell activity and disease development. Such research requires non-invasive techniques to probe and quantify local mechanical properties of cells, namely modulus of elasticity, viscoelastic properties, adhesion, and forces created at the single cell scale.

Many conventional measurements of local mechanical properties of cells use solid probes, such as AFM, thus ignoring that these measured mechanical properties are highly dependent on contact / adhesion between the probe and the cell (the duration of the measurements). On the other hand, the acoustic waves generated by lasers constitute a very suitable tool for probing the mechanical properties of biological cells or tissues in a non-contact and non-invasive configuration.

In conclusion, thanks to the use of a specific surface structuring, we have been able to carry out a study coupling several approaches on a single motor neuron. The mapping of the Brillouin frequency as well as its attenuation makes it possible to identify the structure of the cell, highlighting a nucleus characterized by high rigidity and a lower viscosity than the rest of the cell. The detection of a delayed

acoustic feature with respect to the main echo coupled with direct AFM thickness measurements at the periphery of the cell makes it possible to extract the sound velocity in these areas rich in actin for which the Brillouin oscillation is difficult to analyze. The bulk modulus appears to be greater for this region rich in actin but significantly weaker than that of the nucleus.

3.1 Author contribution statements:

All the authors contributed equally, they carried out the measurements, contributed to the design and implementation of the research, to the analysis of the results and to the writing of the manuscript.

ACKNOWLEDGMENT

The authors would like to thank the help of Sorbonne University Emergence program and Matisse Labex, for their financial contributions in this project gathering INSP and LCMCP.

References

[1] Deok-Ho Kim, Pak Kin Wong, Jungyul Park, Andre Levchenko, and Yu Sun. Microengineered platforms for cell mechanobiology. *Annual Review of Biomedical Engineering*, 11:203–233, 2009.

[2] Robert M. Hochmuth. Micropipette aspiration of living cells. *Journal of Biomechanics*, 33:15–22, 2000.

[3] Thomas D. Brown. Techniques for mechanical stimulation of cells in vitro: a review. *Journal of Biomechanics*, 33:3–14, 2000.

[4] J. A. Hildebrand, D. Rugar, R. N. Johnston, and C. F. Quate. Acoustic microscopy of living cells. *Proc. Nat. Acad. Sci. U.S.A.*, 78:1656–1660, 1981.

[5] T. Kundu. *ultrasonic nondestructive evaluation : engineering and biological material characterization*. CRC Press, 2003.

[6] RA Lemons and CF Quate. Acoustic microscopy: biomedical applications. *Science*, 188(4191):905–911, 1975.

[7] R N Johnston, A Atalar, J Heiserman, V Jipson, and C F Quate. Acoustic microscopy: resolution of subcellular detail. *Proc Natl Acad Sci U S A*, 76(7):3325–3329, Jul 1979.

[8] C. Thomsen, H. T. Grahn, H. J. Maris, and J. Tauc. Surface generation and detection of phonons by picosecond light pulses. *Phys. Rev. B*, 34:4129–4138, Sep 1986.

[9] Jérémie Margueritat, Angélique Virgone-Carlotta, Sylvain Monnier, Hélène Delanoë-Ayari, Hichem C. Mertani, Alice Berthelot, Quentin Martinet, Xavier Dagany, Charlotte Rivière, Jean-Paul Rieu, and Thomas Dehoux. High-frequency mechanical properties of tumors measured by brillouin light scattering. *Phys. Rev. Lett.*, 122:018101, Jan 2019.

[10] C. Rossignol, N. Chigarev, M. Ducousso, B. Audoin, G. Forget, F. Guillemot, and M. C. Durrieu. In vitro picosecond ultrasonics in a single cell. *Applied Physics Letters*, 93(12):123901, 2008.

[11] Fernando Perez-Cota, Richard J. Smith, Hany M. Elsheikha, and Matt Clark. New insights into the mechanical properties of acanthamoeba castellanii cysts as revealed by phonon microscopy. *Biomedical optics express*, 10:2399–2408, May 2019.

[12] Alexis Viel, Emmanuel Péronne, Océane Sénépart, Loïc Becerra, Claire Legay, Fannie Semprez, Léa Trichet, Thibaud Coradin, Ahmed Hamraoui, and Laurent Belliard. Picosecond ultrasounds as elasticity probes in neuron-like cells models. *Applied Physics Letters*, 115(21):213701, 2019.

[13] Sorasak Danworaphong, Motonobu Tomoda, Yuki Matsumoto, Osamu Matsuda, Toshiro Ohashi, Hiromu Watanabe, Masafumi Nagayama, Kazutoshi Gohara, Paul H. Otsuka, and Oliver B. Wright. Three-dimensional imaging of biological cells with picosecond ultrasonics. *Applied physics letters*, 106:163701, 2015.

[14] Liwang Liu, Alexis Viel, Guillaume Le Saux, Laurent Plawinski, Giovanna Muggiolu, Philippe Barberet, Marco Pereira, Cédric Ayela, Hervé Seznec, Marie-Christine Durrieu, Jean-Marc Olive, and Bertrand Audoin. Remote imaging of single cell 3d morphology with ultrafast coherent phonons and their resonance harmonics. *Scientific Reports*, 9(1):6409, 2019.

[15] Fernando Pérez-Cota, Richard J. Smith, Emilia Moradi, Leonel Marques, Kevin F. Webb, and Matt Clark. Thin-film optoacoustic transducers for subcellular brillouin oscillation imaging of individual biological cells. *Applied Optics*, 54:8388, 2015.

[16] Fernando Pérez-Cota, Richard J. Smith, Emilia Moradi, Leonel Marques, Kevin F. Webb, and Matt Clark. High resolution 3d imaging of living cells with sub-optical wavelength phonons. *Scientific Reports*, 6, 2016.

[17] Thomas Dehoux, Maroun Abi Ghanem, Omar F. Zouani, Mathieu Ducousso, Nikolay Chigarev, Clément Rossignol, Nicolas Tsapis, Marie-Christine Durrieu, and Bertrand Audoin. Probing single-cell mechanics with picosecond ultrasonics. *Ultrasonics*, 56:160–171, 2015.

[18] T. Dehoux, M. Abi Ghanem, O. F. Zouani, J.-M. Rampnoux, Y. Guillet, S. Dilhaire, M.-C. Durrieu, and B. Audoin. All-optical broadband ultrasonography of single cells. *Scientific reports*, 5, 2015.

[19] Maroun Abi Ghanem, Thomas Dehoux, Liwang Liu, Guillaume Le Saux, Laurent Plawinski, Marie-Christine Durrieu, and Bertrand Audoin. Opto-acoustic microscopy reveals adhesion mechanics of single cells. *Review of Scientific Instruments*, 89:014901, 2018.

[20] Liwang Liu, Laurent Plawinski, Marie-Christine Durrieu, and Bertrand Audoin. Label-free multiparametric imaging of single cells: dual picosecond optoacoustic microscopy. *Journal of biophotonics*, page e201900045, 2019.

[21] Cyril Jean, Laurent Belliard, Thomas W. Cornelius, Olivier Thomas, Maria Eugenia Toimil-Molares, Marco Cassinelli, Loïc Becerra, and Bernard Perrin. Direct observation of gigahertz coherent guided acoustic phonons in free-standing single copper nanowires. *The Journal of Physical Chemistry Letters*, 5(23):4100–4104, 12 2014.

[22] Cyril Jean, Laurent Belliard, Thomas W. Cornelius, Olivier Thomas, Yan Pennec, Marco Cassinelli, Maria Eugenia Toimil-Molares, and Bernard Perrin. Spatiotemporal imaging of the acoustic field emitted by a single copper nanowire. *Nano Letters*, 16(10):6592–6598, 10 2016.

[23] H G Tattersall. The ultrasonic pulse-echo technique as applied to adhesion testing. *Journal of Physics D: Applied Physics*, 6(7):819–832, may 1973.

[24] M Canillas, B Moreno, E Chinarro, and A M Rajnicek. Tio2 surfaces support neuron growth during electric field stimulation. *Mater Sci Eng C Mater Biol Appl*, 79:1–8, Oct 2017.

[25] Chaim N. Sukenik, Natarajan Balachander, Lloyd A. Culp, Kristine Lewandowska, and Katherine Merritt. Modulation of cell adhesion by modification of titanium surfaces with covalently attached self-assembled monolayers. *Journal of Biomedical Materials Research*, 24(10):1307–1323, 1990.

[26] Kash L. Mittal Alain Carré, editor. *Surface and Interfacial Aspects of Cell Adhesion*. CRC Press, 2011.

[27] Madison L Francis, Shea N Ricketts, Leila Farhadi, Michael J Rust, Moumita Das, Jennifer L Ross, and Rae M Robertson-Anderson. Non-monotonic dependence of stiffness on actin crosslinking in cytoskeleton composites. *Soft Matter*, 15(44):9056–9065, Nov 2019.

[28] Robyn H Pritchard, Yan Yan Shery Huang, and Eugene M Terentjev. Mechanics of biological networks: from the cell cytoskeleton to connective tissue. *Soft Matter*, 10(12):1864–1884, Mar 2014.

[29] Geraldine Rohman, Salah Ramtani, Sylvie Changotade, Credson Langueh, Didier Lutomski, Yves Roussigne, Florent Tetard, Frederic Caupin, and Philippe Djemia. Characterization of elastomeric scaffolds developed for tissue engineering applications by compression and nanoindentation tests, mu-Raman and mu-Brillouin spectroscopies. *Biomedical Optics Express*, 10(4):1649–1659, APR 1 2019.

[30] Benjamin Rappaz, Pierre Marquet, Etienne Cuche, Yves Emery, Christian Depeursinge, and Pierre J. Magistretti. Measurement of the integral refractive index and dynamic cell morphometry of living cells with digital holographic microscopy. *Opt. Express*, 13(23):9361–9373, Nov 2005.

[31] Jonas Binding, Juliette Ben Arous, Jean-François Léger, Sylvain Gigan, Claude Boccara, and Laurent Bourdieu. Brain refractive index measured in vivo with high-na defocus-corrected full-field oct and consequences for two-photon microscopy. *Opt. Express*, 19(6):4833–4847, Mar 2011.

[32] Jingjing Sun, Sung Jin Lee, Lei Wu, Malisa Sarntinoranont, and Huikai Xie. Refractive index measurement of acute rat brain tissue slices using optical coherence tomography. *Opt Express*, 20(2):1084–1095, Jan 2012.

[33] Géraldine Rohman, Salah Ramtani, Sylvie Changotade, Credson Langueh, Didier Lutomski, Yves Roussigné, Florent Tétard, Fréderic Caupin, and Philippe Djemia. Characterization of elastomeric scaffolds developed for tissue engineering applications by compression and nanoindentation tests, μ-raman and μ-brillouin spectroscopies. *Biomedical optics express*, 10(4):1649–1659, 03 2019.